JACS
JOURNAL OF THE AMERICAN CHEMICAL SOCIETY
Article
pubs.acs.org/JACS

A High-Valent Iron–Oxo Corrolazine Activates C–H Bonds via Hydrogen-Atom Transfer

Kevin Cho,[†] Pannee Leeladee,[†] Amanda J. McGown,[†] Serena DeBeer,*[,‡] and David P. Goldberg*[,†]

[†]Department of Chemistry, Johns Hopkins University, 3400 North Charles Street, Baltimore, Maryland 21218, United States
[‡]Department of Chemistry and Chemical Biology, Cornell University, Ithaca, New York 14853, United States, and Max-Planck-Institut für Bioanorganische Chemie, Stiftstrasse 34-36, D-45470 Mülheim an der Ruhr, Germany

Supporting Information

ABSTRACT: Oxidation of the Fe^{III} complex $(TBP_8Cz)Fe^{III}$ [TBP_8Cz = octakis(4-*tert*-butylphenyl)corrolazinate] with O-atom transfer oxidants under a variety of conditions gives the reactive high-valent Fe(O) complex $(TBP_8Cz^{+\bullet})Fe^{IV}(O)$ (**2**). The solution state structure of **2** was characterized by XAS [d(Fe–O) = 1.64 Å]. This complex is competent to oxidize a range of C–H substrates. Product analyses and kinetic data show that these reactions occur via rate-determining hydrogen-atom transfer (HAT), with a linear correlation for log k versus BDE(C–H), and the following activation parameters for xanthene (Xn) substrate: $\Delta H^{\ddagger}$ = 12.7 ± 0.8 kcal mol^{-1}, $\Delta S^{\ddagger}$ = −9 ± 3 cal K^{-1} mol^{-1}, and KIE = 5.7. Rebound hydroxylation versus radical dimerization for Xn is favored by lowering the reaction temperature. These findings provide insights into the factors that control the intrinsic reactivity of Compound I heme analogues.

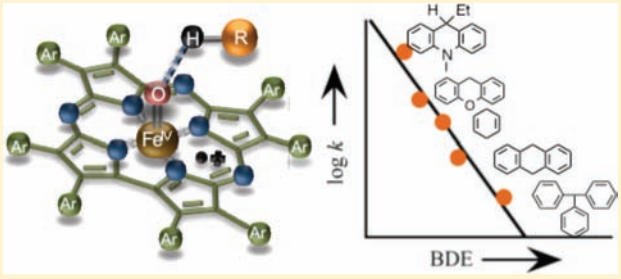

INTRODUCTION

High-valent iron–oxo complexes have been implicated as reactive intermediates in a range of biological transformations and in synthetic catalytic processes. In particular, Fe^{IV}–oxo porphyrin π-cation radical species, designated as Compound I (Cpd-I) in heme proteins (e.g., cytochrome P450), are proposed to mediate many key oxidative processes.[1] Synthetic $Fe^{IV}(O)(porph^{+\bullet})$ complexes are difficult to generate and study because of their instability,[2] but much effort has gone into preparing these and related high-valent metal–oxo complexes because of the potential they offer in helping to define patterns of reactivity and in testing mechanistic hypotheses.[3] Our group has been involved in developing ring-contracted porphyrins known as corrolazines, which are related to the more widely studied corroles. Corrolazines and corroles are designed to stabilize high oxidation states. Although a number of high-valent metal–oxo corrolazines[4] and related corroles[5] have been described, only one example of a metastable mononuclear, high-valent Fe(O) complex has been reported thus far, prepared by our group with an octaaryl-substituted corrolazine.[4d,6]

A few reports have indicated that iron corroles and corrolazines can serve as potent oxidation catalysts, which may utilize one or more high-valent metal–oxo intermediates. The first study of catalysis by a high-valent iron corrole, $(tpfc)Fe^{IV}Cl$ [tpfc = *meso*-tris(pentafluorophenyl)corrolate], was reported by Gross and co-workers.[5i] In this study, $(tpfc)Fe^{IV}Cl$ was shown to be active for catalytic hydroxylation of ethyl benzene and epoxidation of styrene with iodosylbenzene as the sacrificial oxidant. The reactive intermediate of this catalysis is presumed to be a high-valent iron–oxo corrole, although such a species was not characterized. Hayashi and co-workers have been successful in reconstituting the apo forms of horseradish peroxidase (HRP) and myoglobin (Mb) with an iron corrole.[5g] The iron corrole bound in the proteins was catalytically active toward the oxidation of 2-methoxyphenol with hydrogen peroxide as the external oxidant. It is expected that the iron corrole activates hydrogen peroxide to form an HRP or Mb Cpd-I intermediate before reacting with the substrate. However, there has been no characterization of the reactive intermediate in the corrole-reconstituted metalloproteins. Our group has found that $(TBP_8Cz)Fe^{III}$ is also a good catalyst for oxygen-atom transfer and hydroxylation of cyclohexene in organic solution, as well as in the form of nanoparticles [$(TBP_8Cz)Fe^{III}$-NP] in an aqueous environment with pentafluoroiodosobenzene (PFIB) as a sacrificial oxidant.[4d,h] In the former case, there was spectroscopic evidence that indicated a high-valent iron–oxo corrolazine, $(TBP_8Cz^{+\bullet})Fe^{IV}(O)$, is the active intermediate for the oxidation of olefins. For the latter case involving nanoparticles, the catalytic reactivity of $(TBP_8Cz)Fe^{III}$ nanoparticles in an aqueous environment was different compared to that of $(TBP_8Cz)Fe^{III}$ in an organic solution. The catalytic oxidation of cyclohexene with PFIB and $(TBP_8Cz)Fe^{III}$-NP favored the formation of the hydroxylation products over the epoxidation product,[4h] as opposed to the product distribution for the molecular, solution state study. The mechanism of catalytic

Received: December 14, 2011
Published: April 10, 2012

   dx.doi.org/10.1021/ja3018658 | *J. Am. Chem. Soc.* 2012, 134, 7392–7399

oxidations with $(TBP_8Cz)Fe^{III}$-NP may also utilize the same high-valent iron−oxo intermediate as the molecular catalyst, but the nanoparticle architecture and/or the change in solvent (aqueous versus organic) may be responsible for the observed differences in reactivity.

Recently, we have been interested in exploiting the stability of the high-valent iron−oxo corrolazine to examine C−H activation by $(TBP_8Cz^{+\bullet})Fe^{IV}(O)$, a reaction relevant to the proposed mechanism for Cpd-I in heme oxygenases. Herein we describe new, efficient methods of generating this complex for spectroscopic and reactivity studies. These efforts have allowed for the first structural characterization of an Fe(O) corrolazine or corrole by X-ray absorption spectroscopy (XAS). We also provide conclusive evidence for the first time that an Fe(O) corrole-type complex is capable of C−H bond activation, and hydrogen-atom abstraction followed by rebound (or a second H-atom transfer) is the likely mechanism for these reactions, mimicking the proposed reaction course for heme-based oxidations.

EXPERIMENTAL DETAILS

Materials. All reactions were performed using dry solvents and standard Schlenk techniques. The iron(III) corrolazine $(TBP_8Cz)Fe^{III}$ (**1**) and pentafluoroiodosylbenzene were synthesized according to previously published methods.[4d] Dichloromethane, diethyl ether, toluene, and methanol were purified via a Pure-Solv solvent purification system from Innovative Technologies, Inc. *meta*-Chloroperbenzoic acid (mCPBA) was purchased from Sigma-Aldrich, washed with phosphate buffer, and then recrystallized from a CH_2Cl_2/diethyl ether mixture. Xanthene, 9,10-dihydroanthracene (DHA), triphenylmethane (TPM), and ferrocene (Cp_2Fe) were purchased from commercial sources and recrystallized from ethanol. Decamethyl ferrocene (Cp^*_2Fe) was purchased from Sigma-Aldrich and recrystallized from cyclohexane. 9,10-d_2-Xanthene was synthesized according to a literature procedure.[3b] 9,9′-Bixanthene was synthesized as described below. 9-Ethyl-9,10-dihydro-10-methylacridine (AcrHEt) was a gift from S. Fukuzumi.[7] 1,4-Cyclohexadiene (CHD), xanthydrol, eicosane, and anthracene were purchased from commercial sources and used as received.

General Instrumentation. UV−vis spectroscopy was performed on a Varian Cary 50 Bio spectrophotometer, and low-temperature data were collected by using a fiber optic coupler and a Hellma 2 mm quartz immersion probe. Electron paramagnetic resonance (EPR) spectra were recorded on a Bruker EMX EPR spectrometer controlled with a Bruker ER 041 X G microwave bridge at 15 K and equipped with a continuous-flow liquid helium cryostat (ESR900) coupled to a TC503 temperature controller made by Oxford Instruments, Inc. Gas chromatography (GC) was performed on an Agilent 6890N gas chromatograph fitted with an HP-5 (5% phenyl)-methylpolysiloxane capillary column (30 m × 0.32 mm × 0.25 mm) and equipped with a flame-ionization detector. GC-FID response factors for xanthydrol, xanthone, bixanthene, and anthracene were prepared versus eicosane as the internal standard. Temperatures for kinetics were measured by a VWR two-channel thermometer with offsets equipped with both a beaded and stainless steel probe. ^{1}H NMR spectra were recorded on a Bruker AMX-400 spectrometer (400 MHz). Chemical shifts were referenced to the residual solvent peaks.

X-ray Absorption Spectroscopy. XAS data were recorded at the Stanford Synchrotron Radiation Laboratory (SSRL) on focused beamline 9-3, under ring conditions of 3 GeV and 60−100 mA. A Si(220) double-crystal monochromator was used for energy selection, and a Rh-coated mirror (set to an energy cutoff of 10 keV) was used for harmonic rejection. Internal energy calibration was performed by assigning the first inflection point of the Fe foil spectrum to 7111.2 eV. All samples were maintained at 10 K during data collection using an Oxford Instruments CF1208 continuous-flow liquid helium cryostat. Data were measured in fluorescence mode (using a Canberra Ge 30-element array detector). XAS data were measured to k = 11 Å^{-1}. Samples were monitored for photoreduction throughout the course of data collection. Only those scans, which showed no evidence of photoreduction, were used in the final average.

The data were calibrated and averaged using EXAFSPAK.[8] Pre-edge subtraction and splining were conducted using PYSPLINE.[9] A three-region cubic spline of order 2, 3, 3 was used to model the smooth background above the edge. Normalization of the data was achieved by subtracting the spline and normalizing the postedge region to 1. The resultant EXAFS was k^3-weighted to enhance the impact of high-k data.

Theoretical EXAFS signals $c(k)$ were calculated using FEFF (version 7.0)[10] and fit to the data using EXAFSPAK.[8] The nonstructural parameter E_0 was also allowed to vary but was restricted to a common value for every component in a given fit. The structural parameters that were varied during the refinements were the bond distance (R) and the bond variance (s^2). s^2 is related to the Debye−Waller factor, which is a measure of thermal vibration, and to the static disorder of the absorbers and scatterers. Coordination numbers were systematically varied in the course of the analysis, but they were not allowed to vary within a given fit.

Formation of 2 at −78 °C for XAS Spectroscopy. In a one dram vial, **1** was dissolved in 150 μL of toluene (13.3 mM) and cooled to −78 °C. To this solution was added PFIB (50 μL, 0.4 M stock solution in CH_3OH, 10 equiv) to initiate the reaction. The reaction mixture was kept at −78 °C for ∼1 min, upon which a color change from green to dark brown was observed. The sample was then transferred via a precooled pipet to a precooled XAS sample cell and carefully frozen in liquid nitrogen.

Synthesis of 9,9′-Bixanthene. A solution of **1** (0.53 mM) and xanthene (0.53 M) was dissolved in 20 mL of a 1:1 (v/v) CH_2Cl_2/CH_3OH mixture and stirred at room temperature. To this solution was added mCPBA in 20 mg increments up to a total of 80 mg. A transient brown species was observed after each addition. A final addition of 100 mg of mCPBA was then made, causing the green color of **1** to fade to yellow. The solvent was removed in vacuo. The crude reaction mixture was purified by column chromatography [silica gel, 2:1 (v/v) hexane/CH_2Cl_2 mixture], yielding 9,9′-bixanthyl as a white solid (11.8 mg, 3%): ^{1}H NMR (CD_2Cl_2) δ 7.21 (t, J = 7.60 Hz, 4H), 6.95 (t, J = 7.36 Hz, 4H), 6.83 (d, J = 8.16 Hz, 4H), 6.70 (d, J = 7.52 Hz, 4H), 4.26 (s, 2H).[11]

Formation of $(TBP_8Cz^{+\bullet})Fe^{IV}(O)$ (2) with mCPBA at −78 °C. In a typical experiment, a solution of **1** was prepared under Ar in 5.0 mL of a 1:1 (v/v) CH_2Cl_2/CH_3OH mixture (80 μM) in a custom-made Schlenk flask fitted with a quartz immersion probe and attached to a UV−vis spectrophotometer via a fiber optics coupler. The solution was cooled to −78 °C, and mCPBA (100 μL, 4 mM stock solution in a 1:1 CH_2Cl_2/MeOH mixture, 1 equiv) was added to the reaction mixture. The reaction mixture changed color from green to brown after the addition of oxidant. The temperature was maintained at −78 °C, and the reaction showed isosbestic conversion from **1** (λ_{max} = 440, 611, and 747 nm) to **2** (λ_{max} = 396, 730, and 843 nm) with isosbestic points at 394 and 770 nm determined by UV−vis spectroscopy. The reaction was monitored until complete formation of **2** [λ_{max} = 396 nm (ε = 3.8 × 10^4), 730 nm (ε = 3.9 × 10^3), and 843 nm (ε = 1.6 × 10^3)] was observed.

Reaction of 2 with Cp_2Fe and Cp^*_2Fe. Formation of **2** at −78 °C was conducted as described above. The solution containing **2** (0.08 mM) was titrated with Cp_2Fe or Cp^*_2Fe (6.4 mM stock solution in a 1:1 CH_2Cl_2/MeOH mixture). Cp_2Fe or Cp^*_2Fe was added in 0.4 equiv increments in 25 μL of CH_2Cl_2 for each addition up to a total of 4 equiv. After each addition, an immediate change was observed by UV−vis spectroscopy up to 2 equiv, at which point no further change in the spectrum was noted. A color change from brown to green was observed as **2** was reduced to **1**.

Reaction of 2 and DHA for Product Analysis. In a typical reaction, a solution of **1** (16 μM) and DHA (16 mM) was dissolved under Ar in 90 mL of a 1:1 (v/v) CH_2Cl_2/MeOH mixture. To this solution was added mCPBA (200 μL, 14 mM stock solution in a 1:1 CH_2Cl_2/MeOH mixture, 1 equiv). The reaction mixture instantly

dx.doi.org/10.1021/ja3018658 | J. Am. Chem. Soc. 2012, 134, 7392−7399

turned brown and then slowly returned to a green color. After ~30 min, the solvent was removed under vacuum to dryness, and the solid was redissolved in 500 μL of CH_2Cl_2 with eicosane added as an internal standard. The reaction mixture was directly injected onto the gas chromatograph for analysis. The product, anthracene, was identified by GC in comparison with an authentic sample and quantitated by integration and comparison with an eicosane calibration curve. The yield was obtained from an average of three runs.

Reaction of 2 and Xanthene for Product Analysis. A solution of **1** (1.2 mM) and xanthene (60 mM) was prepared under Ar in a 1:1 (v/v) CH_2Cl_2/MeOH mixture (500 μL) at room temperature or −25 °C. To this solution was added mCPBA (100 μL, 6 mM stock solution in a 1:1 CH_2Cl_2/MeOH mixture, 1 equiv). The reaction mixture instantly turned brown, followed by a rapid return to a green color. A solution of eicosane was added as an internal standard, and the reaction mixture was directly injected onto the gas chromatograph for analysis. The products, xanthydrol and 9,9′-bixanthyl, were identified by GC in comparison to authentic samples and quantitated by integration and comparison with eicosane calibration curves. Yields were obtained from an average of two runs.

Kinetics. In a typical experiment, a mixture of **1** (16 μM) and C−H substrate (AcrHEt, xanthene, 9,10-d_2-xanthene, DHA, CHD, or TPM from 0.12 to 240 mM) was dissolved in 5 mL of a 1:1 (v/v) CH_2Cl_2/CH_3OH solution in a custom quartz cuvette fitted with a 100 mL round-bottom Schlenk flask. To this solution was added mCPBA (100 μL, 0.8 mM stock solution in a 1:1 CH_2Cl_2/MeOH mixture, 1 equiv), and the solution was mixed by hand for <5 s. A color change occurred immediately after the addition of oxidant from green to brown associated with the conversion of **1** (λ_{max} = 440, 611, and 747 nm) to **2** (λ_{max} = 397, 730, and 843 nm). Immediately after the solution had been mixed, the reaction was monitored by UV−vis spectroscopy until no further change in the spectrum was observed. Each substrate reaction resulted in a color change from brown **2** to the green color of starting Fe^{III} complex **1**. The pseudo-first-order rate constants, k_{obs}, were obtained from nonlinear fitting of the growth in absorbance at 440 nm versus time (t) by eq 1, where Abs_f is the final absorbance and Abs_0 is the initial absorbance.

$$Abs_t = Abs_f - (Abs_f - Abs_0)e^{(-k_{obs}t)} \quad (1)$$

The reaction was repeated for all substrates over a range of at least three different concentrations. The plot of k_{obs} versus substrate concentration was found to be linear for each substrate. Second-order rate constants (k) were obtained from the slope of the best-fit lines. The kinetic isotope effect (KIE) of xanthene was obtained from the second-order rate constants of xanthene (k_H) and 9,10-d_2-xanthene (k_D) as shown in eq 2.

$$KIE_{xanthene} = \frac{k_H}{k_D} \quad (2)$$

BDE(C−H) values for xanthene, CHD, DHA, and TPM were obtained from ref 12. The BDE(C−H) value for AcrHEt was obtained from eq 3, where $\Delta E_{AcrHEt-AcrEt^\bullet}$ (393.1 kcal mol^{-1}) and $\Delta E_{AcrH_2-AcrH^\bullet}$ (392.3 kcal mol^{-1}) were calculated from DFT with a B3LYP/6-31+(d,p) basis set and the experimental value for BDE(C−H) of $AcrH_2$ (73.7 kcal mol^{-1}) was obtained from ref 13.

$$BDE_{AcrHEt} - BDE_{AcrH_2} = \Delta E_{AcrHEt-AcrEt^\bullet} - \Delta E_{AcrH_2-AcrH^\bullet} \quad (3)$$

Temperature Dependence of the Rate of the Reaction of 2 and Xanthene (−35 to 22 °C). In a typical experiment, $(TBP_8Cz)Fe^{III}$ was dissolved in 5 mL of a 1:1 (v/v) CH_2Cl_2/CH_3OH solution (80 μM) in a custom-made Schlenk flask fitted with a quartz immersion probe and attached to a UV−vis spectrophotometer via a fiber optics coupler. The solution was cooled to −35 °C, and mCPBA (100 μL, 4 mM stock solution in a CH_2Cl_2/MeOH mixture, 1 equiv) was added to the mixture. The reaction mixture was magnetically stirred, and the reaction temperature was maintained within ±0.5 °C. The isosbestic conversion of **1** (λ_{max} = 440, 611, and 747 nm) to **2** (λ_{max} = 385, 730, and 843 nm) was monitored by UV−vis spectroscopy until no further change in the spectrum was observed. Excess xanthene dissolved in CH_2Cl_2 (0.1−1.2 mM) was added to the stirring solution. The change in absorbance at 440 nm was observed over time by UV−vis spectroscopy. The pseudo-first-order rate constants, k_{obs}, and second-order rate constants at each temperature were obtained as described above. Activation parameters were determined from the linear fit of $\ln(k/T)$ versus $1/T$ and the Eyring equation (eq 4).[14]

$$\ln\left(\frac{k}{T}\right) = -\left(\frac{\Delta H^{\ddagger}}{R}\right)\left(\frac{1}{T}\right) + \frac{\Delta S^{\ddagger}}{R} + \ln\frac{k_b}{h} \quad (4)$$

RESULTS AND DISCUSSION

In a previous report, we showed that the quantitative oxidation of the Fe^{III} complex **1** (λ_{max} = 440, 611, and 747 nm) shown in Scheme 1 could be accomplished by the addition of 1 equiv of

Scheme 1

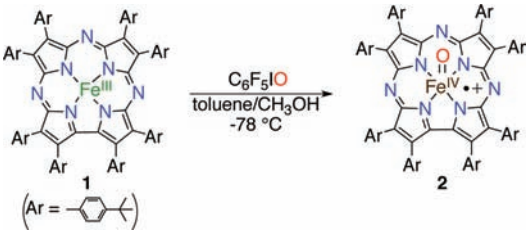

pentafluoroiodosylbenzene (PFIB) in a CH_2Cl_2/MeOH mixture at −78 °C, giving isosbestic conversion to a metastable brown product (λ_{max} = 396, 730, and 843 nm).[4d] The low-temperature UV−vis and EPR data, along with redox titrations and oxygen-atom transfer reactivity, provided evidence of the assignment of **2** as the high-valent iron−oxo complex $[(TBP_8Cz^{+\bullet})Fe^{IV}(O)]$, a corrolazine analogue of Cpd-I. However, no direct structural information about **2** was obtained. We sought to characterize **2** by X-ray absorption spectroscopy (XAS) to obtain information about the solution state structure and iron oxidation state of samples of **2** generated at low temperatures.

XAS Studies. The generation of **2** in a CH_2Cl_2/MeOH mixture was not practical for XAS because of the strong absorption background from the chlorinated solvent. Oxidation of **1** with PFIB in a toluene/MeOH mixture at −78 °C to afford **2** (Scheme 1) proceeded with the same isosbestic conversion (isosbestic points at 394, 500, and 770 nm) and gave the same EPR spectrum that was seen previously in a CH_2Cl_2/MeOH mixture (Figure 1).[4d] The X-ray absorption spectrum in the near-edge region for **2** in a toluene/MeOH mixture is shown in Figure 2. The energy of the rising Fe K-edge is dependent upon both oxidation state and structure. The edge energy of 7124 eV for **2** is characteristic of reported low-spin (S = 1) Fe^{IV} complexes.[15−17] As seen in Figure 2, **2** is shifted by ~1 eV to a higher energy in comparison to that of the Fe^{III} starting material. In addition, an intense pre-edge feature (~7113 eV) is seen for complex **2** that is significantly more intense than that seen for complex **1**. This peak is attributed primarily to a 1s → (M_{3dz^2}) transition, which gains intensity because of the increased level of metal 4p mixing induced by M−L overlap.[18] The increase in the intensity of this pre-edge feature is a hallmark of terminal, M═X multiply bonded complexes (X = O or N) and provides strong evidence of the presence of the terminal oxo ligand in **2**.[4g] Best fits to the EXAFS data (Figure 2 and Table 1) for **2** are obtained with

dx.doi.org/10.1021/ja3018658 | J. Am. Chem. Soc. 2012, 134, 7392−7399

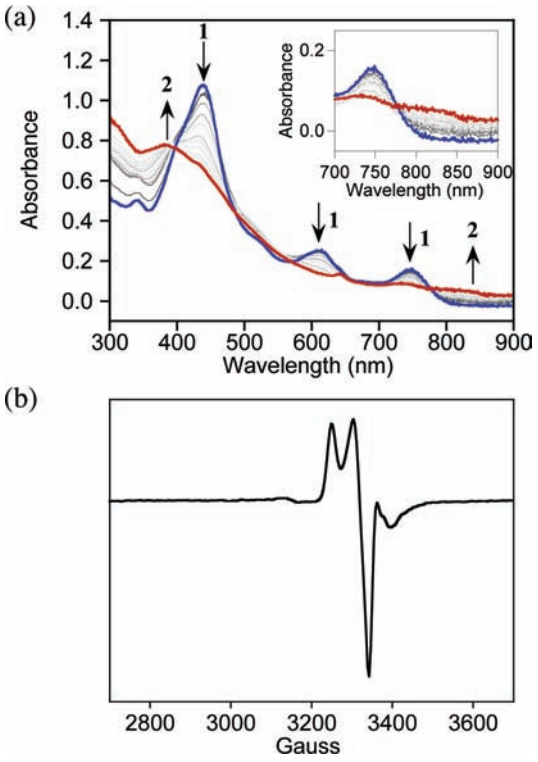

Figure 1. (a) UV–vis spectra of the reaction of **1** (blue line) with 10 equiv of PFIB to give **2** (red line) in a toluene/MeOH mixture (3:1, v/v) at −78 °C. (b) X-Band EPR spectrum at 15 K of **1** and PFIB in a toluene/MeOH mixture (3:1, v/v). Experimental conditions: frequency, 9.48 GHz; microwave power, 2.01 mW; modulation frequency, 100 kHz; modulation amplitude, 10.0 G.

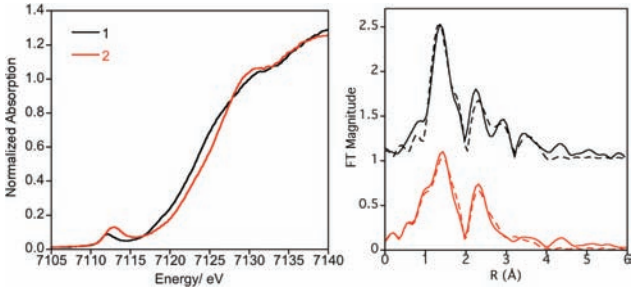

Figure 2. Comparison of the Fe K-edge XAS data for **1** and **2** (left). Fourier transforms of the Fe K-edge EXAFS data (solid lines) and the corresponding fits (dashed lines) for **1** (black) and **2** (red) (right).

Table 1. EXAFS Fit Results for 1 and 2

	1		2	
	R (Å)	σ^2 (Å^2)	R (Å)	σ^2 (Å^2)
4 Fe–N	1.85	0.0011	1.84	0.0026
1 Fe–O	–	–	1.64	0.0010
4 Fe–C	2.88	0.0073	2.87	0.0049
16 Fe–C	3.15	0.0019	3.12	0.0115
16 Fe–C	4.24	0.0107	4.15	0.0163
ΔE_0	−15.4		−15.1	
error[a]	0.35		0.21	

[a]The error is given by $\sum[(\chi_{obsd} - \chi_{calcd})^2 k^6]/\sum(\chi_{obsd}{}^2 k^6)$.

four N donors at 1.84 Å and one O donor at a short distance of 1.64 Å (Table 1). Without the inclusion of the short Fe–O vector, the fit error value increases significantly (from 0.21 to 0.65). Importantly, no similar short vector can be fit to ferric precursor **1** (Table 1). The EXAFS data thus confirm the presence of a multiply bonded terminal oxo group in **2**, with a d(Fe–O) of 1.64 Å that is in excellent agreement with Fe–O distances reported for Fe^{IV}(O) porphyrins[15] and nonheme Fe^{IV}(O) complexes.[17] Thus, the XAS data fully support the assignment of **2** as a Cpd-I analogue.

Generation of 2 with mCPBA. With the assignment of **2** as an iron–oxo complex confirmed by XAS, we sought to examine its reactivity toward C–H bond cleavage. The generation of **2** with PFIB at −78 °C was useful for spectroscopic characterization but was prohibitively slow (12–14 h for completion), preventing the practical examination of reactions of **2**. We therefore sought a method that would result in the more rapid formation of **2** and examined the stronger oxidant mCPBA for this purpose. Addition of 1.0 equiv of mCPBA to **1** at −78 °C (Scheme 2) led to the generation of **2** in 1 min as seen by UV–vis spectroscopy (Figure 3a). The final spectrum (red) in Figure 3a matches that

Scheme 2

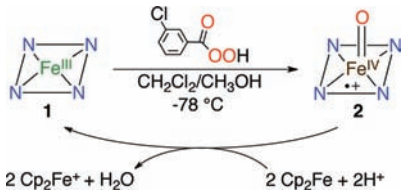

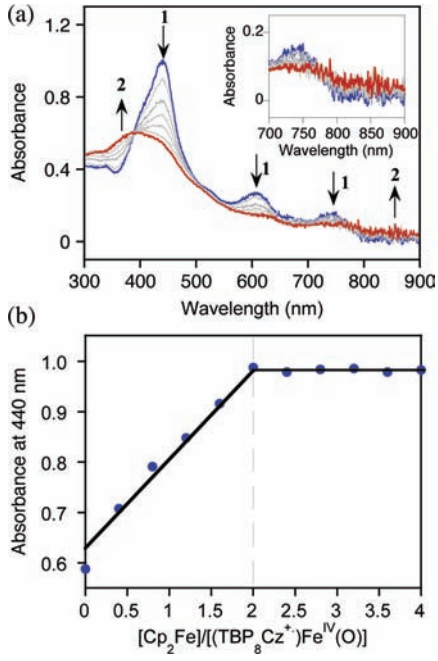

Figure 3. (a) UV–vis spectral changes for the reaction of **1** and mCPBA (1 equiv) at −78 °C to give **2**. (b) Changes in absorbance at 440 nm for **1** as a function of the ratio of reductant to **2**.

seen for the product of oxidation of **1** with PFIB. Care must be taken to employ a stoichiometric amount of mCPBA, because the addition of even a small excess of this oxidant leads to significant decomposition of the iron corrolazine. EPR spectroscopy of **2** generated via mCPBA oxidation revealed a spectrum similar to that seen for **2** from PFIB, although a

dx.doi.org/10.1021/ja3018658 | J. Am. Chem. Soc. 2012, 134, 7392–7399

radical impurity appears to overlap with the signal in the $g = 2$ region (Figure S2 of the Supporting Information).

Complex **2** is stable at −78 °C but shows rapid reduction back to **1** upon addition of the one-electron reductant Cp_2Fe or Cp^*_2Fe. Spectral titration with the ferrocene derivatives (Figure 3b) led to the smooth regeneration of the Fe^{III} complex (Figure S2 of the Supporting Information). The titration shows that 2 equiv of reductant is required for the quantitative conversion of **2** to **1**, confirming that **2** behaves as a $2e^-$ oxidant and is two oxidation levels above **1**, as expected for an $Fe^{IV}(O)$ π-cation radical complex. Isosbestic conversion was observed for the reactions with the ferrocene derivatives, indicating that the one-electron-reduced intermediate $[(TBP_8Cz)Fe^{IV}(O)]^-$ does not build up to any extent. These results imply a mechanism in which the first reduction step is rate-determining. Both reduction steps are also likely to be accompanied by protonation at the terminal oxo position. This mechanism is the same as that described for the reduction of (TBP_8Cz)-$Mn^V(O)$ with ferrocene derivatives.[4i]

Notably, we found that mCPBA could also be used at room temperature (22 °C) to generate **2**. Reactions at room temperature with a stoichiometric amount of PFIB as the oxidant led to insufficient buildup of **2** because of rapid decay back to **1**. When excess PFIB was employed to increase the oxidation rate, significant decomposition (bleaching) of **1** was noted by UV−vis spectroscopy. However, oxidation of **1** by mCPBA was sufficiently fast at 22 °C to give a reasonable buildup of **2** prior to the decay and partial return of **1** (Figure S3 of the Supporting Information). These results suggested that **2** could be generated in situ at room temperature in the presence of potential substrates.

C−H Bond Activation. Treatment of **1** with 1 equiv of mCPBA in the presence of excess 9,10-dihydroanthracene (DHA, 1000 equiv) in a CH_2Cl_2/MeOH mixture at 22 °C led to the rapid formation of **2** as seen by UV−vis spectroscopy, followed by conversion of **2** back to **1** (73% recovery of **1** based on absorbance at 440 nm). Product analysis of the reaction of **2** and DHA under Ar by GC-FID showed the production of anthracene in good yield (74%), without any evidence of other oxidation products (i.e., anthrone, anthraquinone, or anthracene dimer) (Scheme 3). These data show that **2** is a

Scheme 3

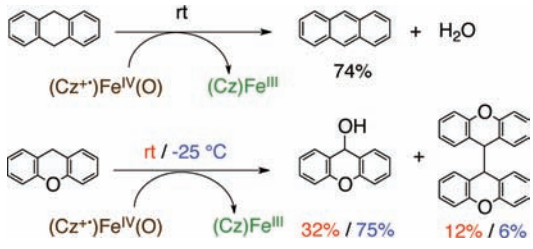

competent oxidant for DHA, and the production of anthracene is consistent with two consecutive hydrogen-atom abstractions, as expected for the two oxidizing equivalents of **2**. Control reactions with mCPBA showed no anthracene product under the same conditions.

Addition of xanthene, an alternative substrate with a BDE(C−H) similar to that of DHA, also resulted in the rapid conversion of **2** to **1** as determined by UV−vis spectroscopy. Product analysis revealed xanthydrol (32%) and 9,9′-bixanthene (12%) as the major oxidation products (Scheme 3). Although these products were consistent with direct oxidation of xanthene by **2** under strict anaerobic conditions, the combined yield based on total oxidizing equivalents for **2** was modest (44%). We speculated that the modest yield was due to the competing background decay of **2** in this case. To enhance the stability of **2**, xanthene oxidation was examined at a lower temperature (−25 °C). The combined yield of xanthydrol and 9,9′-bixanthene was significantly improved, to 81% at −25 °C. Interestingly, there was also a dramatic change in product distribution, with 75% xanthydrol and 6% 9,9′-bixanthene formed at −25 °C.

Kinetics. To gain insight into the mechanism of C−H bond oxidation by **2**, we performed several kinetic experiments. A series of C−H substrates with a range of BDE(C−H) values were reacted with **2** under pseudo-first-order conditions, and rates of reaction were measured by UV−vis spectroscopy. The representative time-resolved UV−vis spectra for the reaction with cyclohexadiene are shown in Figure 4, together with the

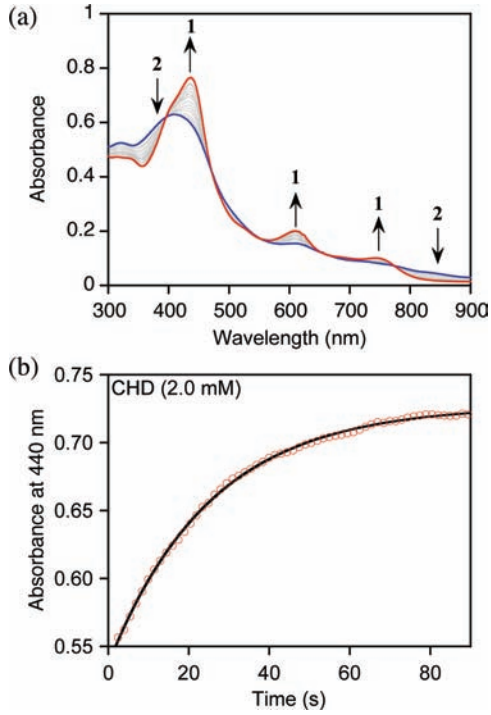

Figure 4. (a) Time-resolved UV−vis spectra of the reaction of **2** (16 μM) with excess CHD (2.0 mM), in a CH_2Cl_2/MeOH mixture (1:1, v/v, 5 mL) at 22 ± 1 °C. (b) Change in absorbance at 440 nm vs time corresponding to the growth of **1** for the data in panel a.

first-order curve for this reaction. Good first-order kinetics were observed for each of the substrates up to five half-lives, yielding k_{obs} values that correlated linearly with substrate concentration (Figure S4 of the Supporting Information). The derived second-order rate constants were plotted versus BDE(C−H) values for each substrate, and a linear relationship was found with a slope of −0.42, as shown in Figure 5a. The slope in Figure 5a also matches that seen for a porphyrin Cpd-I analogue recently reported by Nam and Shaik, $[(tmp)^{+\bullet}Fe^{IV}(O)(p\text{-X-PyO})]^+$ (slope of −0.43),[3b,19] as well as $Mn^V(O)$ corrolazines (slope of −0.42 to −0.62).[4e] In addition, a significant kinetic isotope effect (KIE = 5.7) for xanthene/9,10-d_2-xanthene was observed (Figure 5b). Taken together, these data provide strong support for a mechanism that

dx.doi.org/10.1021/ja3018658 | J. Am. Chem. Soc. 2012, 134, 7392−7399

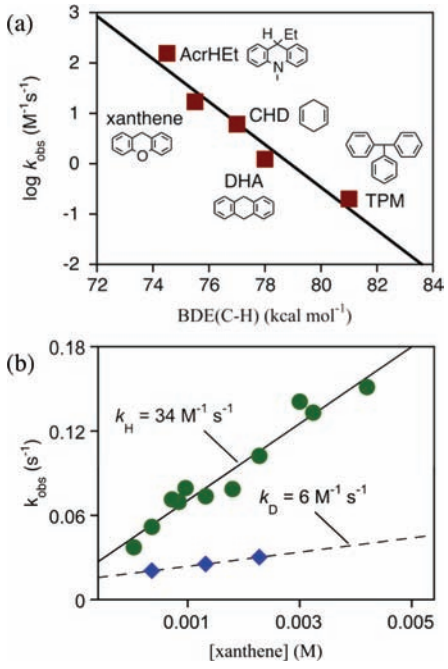

Figure 5. (a) Dependence of the log k values for the reaction of **2** with C−H substrates on the BDE values of the scissile C−H bond,[12] where k values are normalized per reactive C−H bond. (b) Second-order plots for xanthene [green circles (experiment), solid line (fit)] and 9,10-d_2-xanthene [blue diamonds (experiment), dashed line (fit)].

involves HAT between the substrate C−H bond and **2** as the rate-determining step. A similar conclusion has been reached previously regarding the mechanism of $(TBP_8Cz)Mn^V(O)$ and O−H and C−H substrate oxidations.[4e,f]

The relative stability of **2** at moderate temperatures (−35 °C to room temperature) gave us the ability to measure activation parameters for C−H activation. The temperature dependence of the rate constants for the reaction of **2** with xanthene was examined from −35 to 22 °C (Figure S5 of the Supporting Information), and an Eyring plot was constructed as shown in Figure 6. The plot is nicely linear and yields a $\Delta H^{\ddagger}$ of 12.7 ± 0.8 kcal mol^{-1} and a $\Delta S^{\ddagger}$ of −9 ± 3 cal K^{-1} mol^{-1}. A direct comparison with **2** generated from PFIB at −25 °C showed no significant change in the rate constant for oxidation of xanthene, indicating that the identity of the oxidant has no

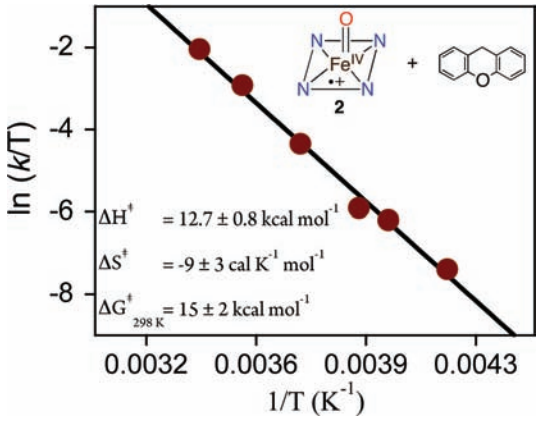

Figure 6. Temperature dependence of the rate constants for xanthene plotted as ln(k/T) vs 1/T.

influence on the kinetic parameters. These data provide some of the first activation parameters for an $Fe^{IV}(O)$ porphyrinoid π-cation radical participating in C−H activation.[20] Limited data are available for other high-valent M=O complexes and C−H substrates. Our $\Delta H^{\ddagger}$ value falls in the range reported for abstraction of a hydrogen from C−H substrates by Ru−oxo, Mn−oxo, and nonheme Fe−oxo complexes.[21] The negative activation entropy observed for **2** is consistent with a bimolecular, second-order process but is relatively high (more positive) compared to those of the former complexes. This $\Delta S^{\ddagger}$ value suggests a less constrained transition state for **2** and xanthene, keeping the overall barrier ($\Delta G^{\ddagger}_{298}$ = 15 ± 2 kcal mol^{-1}) relatively low.

A proposed mechanism to account for all of the observations regarding the reaction of **2** with C−H substrates is illustrated in Scheme 4 for the reaction between **2** and xanthene. An initial

Scheme 4. Proposed Mechanism of C−H Bond Activation

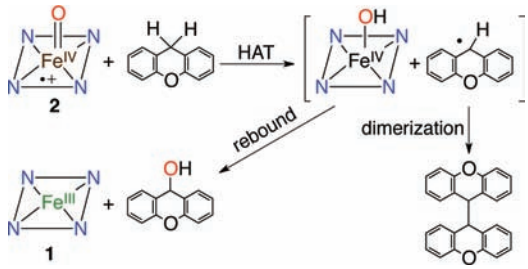

HAT step yields an $Fe^{IV}(OH)$ intermediate along with the xanthyl radical ($Xn^{\bullet}$). At this point, there are two possible reaction pathways, one in which a rebound step occurs to give the alcohol and the other in which cage escape of $Xn^{\bullet}$ is followed by dimerization to give the radical coupled product. The isosbestic conversion of **2** to **1** upon reaction with the C−H substrates indicates that the proposed $Fe^{IV}(OH)$ intermediate does not build up to any measurable extent over the course of the reaction. This observation is consistent with hydroxylation via a fast rebound step being the dominant pathway, which prevents the buildup of $Fe^{IV}(OH)$ and minimizes cage escape of the xanthyl radical.[22] In the dimerization pathway, the $Fe^{IV}(OH)$ intermediate either reacts with another molecule of Xn to generate $Xn^{\bullet}$ and $Fe^{III}(OH_2)$ or possibly decays through an unknown decomposition step. Similarly, the oxidation of DHA likely goes through an initial HAT step, but instead of rebound hydroxylation, the $Fe^{IV}(OH)$ intermediate can immediately abstract a second H atom from the DHA radical, giving the dehydrogenated anthracene product. If cage escape for $DHA^{\bullet}$ occurs, it likely rapidly loses the second $H^{\bullet}$ to **2** or another $Fe^{IV}(OH)$ intermediate, because no evidence of dimerization of $DHA^{\bullet}$ was obtained. This result is not surprising given the very weak C−H bond of $DHA^{\bullet}$ [BDE(C−H) = 43 kcal mol^{-1}].[21a] The dramatic change in product ratios with temperature for xanthene oxidation may also be explained within the context of the mechanism in Scheme 4. A large shift toward production of xanthydrol at −25 °C may be explained by suppression at low temperatures of the bimolecular radical dimerization pathway versus the rebound step in Scheme 4.

Comparison of 2 to Other Cpd-I Analogues. It is of interest to compare the intrinsic reactivity of **2** with that of porphyrin Cpd-I analogues. A recent study of $[(TMP)^{+\bullet}Fe^{IV}(O)(p\text{-X-PyO})]^{+}$ reports rate constants for

dx.doi.org/10.1021/ja3018658 | J. Am. Chem. Soc. 2012, 134, 7392−7399

xanthene that are approximately 50−225 times larger than that found for **2**.[3b] The greater reactivity of the tmp complex may, to a first approximation, be assigned to the differences in charge between porphyrin and corrolazine, where the extra negative charge provided by the corrolazine ligand reduces the electrophilicity of **2** (a neutral complex) in comparison to that of the cationic $[(TMP)^{+\bullet}Fe^{IV}(O)]^{+}$. In support of this, recent work from Groves on a tmp derivative bearing four positively charged methylpyridinium *meso* substituents showed that it reacts with a rate constant $\sim 10^5$ times higher than that of the parent tmp complex in xanthene oxidation.[3a] However, differences in charge are only one aspect that may influence the reactivity of high-valent metal−oxo porphyrinoid compounds. The much greater reactivity for the former methylpyridinium derivative may be due to the strong electron withdrawing properties of the *meso* substituents and their consequential effect on the redox potential of the central iron.[2] Possible spin state crossing phenomena may also be involved in enhancing the reactivity.[3a] In fact, we have shown that the addition of negatively charged axial ligands (X^-) to neutral $[(TBP_8Cz)Mn^{V}(O)]^{0}$ greatly increases its reactivity toward C−H substrates.[4e] This effect was attributed to an increase in the basicity (i.e., the pK_a) of the metal−oxo unit, similar to the proposed influence of the anionic thiolate donor *trans* to the ferryl−oxo unit in Cyt-P450.[23] These previous results, taken together with the findings presented here, suggest that simple differences in charge do not readily explain all of the reactivity trends, and a number of other factors can influence the reactivity of high-valent iron−oxo porphyrinoid complexes.[24]

The stabilization of high-valent oxidation states by trianionic corroles has been attributed to the increase in the energy of the d orbitals relative to other porphyrin derivatives. This increase results in the energy of the metal d orbitals being raised above the ligand HOMO, thus allowing for the stabilization of high oxidation states and causing a consequent reduction in reactivity.[5m] The corrolazine ligand may have a similar influence on the d orbital manifold, helping to stabilize the high-valent Fe−oxo intermediate and as a result lowering the reaction rates for C−H activation.

CONCLUSIONS

In summary, we have generated a Cpd-I analogue with a corrole-type framework and conducted the first structural characterization of such a species by XAS. This complex is competent to oxidize a range of C−H substrates, and a concerted HAT mechanism for the key C−H activation step is strongly indicated by the data. A rare assessment of the activation parameters for C−H activation by a high-valent Fe(O) complex was also obtained. In the case of xanthene, a dominant rebound mechanism that leads to a hydroxylated product was found, akin to hydroxylation by Cpd-I in Cyt-P450. The efficiency of this step is significantly enhanced over that of radical dimerization by lowering the reaction temperature, an effect that to the best of our knowledge has not been reported before for high-valent Fe(O) complexes. Finally, the overall reactivity of **2** was shown to be lower than that of porphyrin Cpd-I analogues. Several factors, including charge considerations, may be responsible for the difference in reactivity. Other effects such as spin state crossing and the electron withdrawing nature of the substituents have also been implicated in the reactivity of Cpd-I species,[2d,e,3a] and future calculations will help shed light on these issues.

ASSOCIATED CONTENT

Supporting Information

Spectroscopic and kinetic data (Figures S1−S5). This material is available free of charge via the Internet at http://pubs.acs.org.

AUTHOR INFORMATION

Corresponding Author

dpg@jhu.edu; serena.debeer@mpi-mail.mpg.de

Notes

The authors declare no competing financial interest.

ACKNOWLEDGMENTS

This work was supported by the National Science Foundation (Grant CHE0909587 to D.P.G.) and a seed grant from the Environment, Energy, Sustainability & Health Institute of The Johns Hopkins University. S.D. thanks Cornell University, the Alfred P. Sloan Foundation, and the Max Planck Society for funding. Portions of this research were conducted at SSRL, SLAC, a user facility operated by the U.S. Department of Energy (DOE) and Stanford University. The SSRL SMB Program is supported by the DOE, OBER, and the National Institutes of Health. We are grateful to S. Fukuzumi for a gift of 9-ethyl-9,10-dihydro-10-methylacridine. P.L. is grateful for the Queen Sirikit Scholarship (Thailand).

REFERENCES

(1) (a) Shaik, S.; Kumar, D.; de Visser, S. P.; Altun, A.; Thiel, W. *Chem. Rev.* **2005**, *105*, 2279−2328. (b) Meunier, B.; de Visser, S. P.; Shaik, S. *Chem. Rev.* **2004**, *104*, 3947−3980. (c) Rittle, J.; Green, M. T. *Science* **2010**, *330*, 933−937. (d) Makris, T. M.; von Koenig, K.; Schlichting, I.; Sligar, S. G. *J. Inorg. Biochem.* **2006**, *100*, 507−518. (e) Groves, J. T. *Proc. Natl. Acad. Sci. U.S.A.* **2003**, *100*, 3569−3574.

(2) (a) McLain, J. L.; Lee, J.; Groves, J. T. In *Biomimetic Oxidations Catalyzed by Transition Metal Complexes*; Meunier, B., Ed.; Imperial College Press: Cambridge, U.K., 2000; Chapter 3, pp 91−169. (b) Ostovic, D.; Bruice, T. C. *Acc. Chem. Res.* **1992**, *25*, 314−320. (c) Groves, J. T. *J. Inorg. Biochem.* **2006**, *100*, 434−447. (d) Nam, W. *Acc. Chem. Res.* **2007**, *40*, 522−531. (e) Goh, Y. M.; Nam, W. *Inorg. Chem.* **1999**, *38*, 914−920.

(3) (a) Bell, S. R.; Groves, J. T. *J. Am. Chem. Soc.* **2009**, *131*, 9640−9641. (b) Kang, Y.; Chen, H.; Jeong, Y. J.; Lai, W.; Bae, E. H.; Shaik, S.; Nam, W. *Chem.—Eur. J.* **2009**, *15*, 10039−10046. (c) Hessenauer-Ilicheva, N.; Franke, A.; Wolak, M.; Higuchi, T.; van Eldik, R. *Chem.—Eur. J.* **2009**, *15*, 12447−12559. (d) Hessenauer-Ilicheva, N.; Franke, A.; Meyer, D.; Woggon, W.-D.; van Eldik, R. *Chem.—Eur. J.* **2009**, *15*, 2941−2959. (e) Parsell, T. H.; Yang, M. Y.; Borovik, A. S. *J. Am. Chem. Soc.* **2009**, *131*, 2762−2763. (f) Yin, G. C.; Danby, A. M.; Kitko, D.; Carter, J. D.; Scheper, W. M.; Busch, D. H. *J. Am. Chem. Soc.* **2007**, *129*, 1512. (g) Garcia-Bosch, I.; Company, A.; Cady, C. W.; Styring, S.; Browne, W. R.; Ribas, X.; Costas, M. *Angew. Chem., Int. Ed.* **2011**, *50*, 5648−5653. (h) Kurahashi, T.; Kikuchi, A.; Shiro, Y.; Hada, M.; Fujii, H. *Inorg. Chem.* **2010**, *49*, 6664−6672. (i) Jeong, Y. J.; Kang, Y.; Han, A. R.; Lee, Y. M.; Kotani, H.; Fukuzumi, S.; Nam, W. *Angew. Chem., Int. Ed.* **2008**, *47*, 7321−7324.

(4) (a) Goldberg, D. P. *Acc. Chem. Res.* **2007**, *40*, 626−634. (b) Kerber, W. D.; Goldberg, D. P. *J. Inorg. Biochem.* **2006**, *100*, 838−857. (c) McGown, A. J.; Badiei, Y. M.; Leeladee, P.; Prokop, K. A.; DeBeer, S.; Goldberg, D. P. In *Handbook of Porphyrin Science*; Kadish, K. M., Smith, K. M., Guilard, R., Eds.; World Scientific Press: Singapore, 2011; Vol. *14*, pp 525−599. (d) McGown, A. J.; Kerber, W. D.; Fujii, H.; Goldberg, D. P. *J. Am. Chem. Soc.* **2009**, *131*, 8040−8048. (e) Prokop, K. A.; de Visser, S. P.; Goldberg, D. P. *Angew. Chem., Int. Ed.* **2010**, *49*, 5091−5095. (f) Lansky, D. E.; Goldberg, D. P. *Inorg. Chem.* **2006**, *45*, 5119−5125. (g) Lansky, D. E.; Mandimustra, B.; Ramdhanie, B.; Clausén, M.; Penner-hahn, J.; Zvyagin, S. A.; Tesler, J.; Krzystek, J.; Zhan, R.; Ou, Z.; Kadish, K. M.; Zakharov, L.; Rheingold,

A. L.; Goldberg, D. P. *Inorg. Chem.* **2005**, *44*, 4485−4498. (h) Cho, K.; Kerber, W. D.; Lee, S. R.; Wan, A.; Batteas, J. D.; Goldberg, D. P. *Inorg. Chem.* **2010**, *49*, 8465−8473. (i) Fukuzumi, S.; Kotani, H.; Prokop, K. A.; Goldberg, D. P. *J. Am. Chem. Soc.* **2011**, *133*, 1859−1869.

(5) (a) Gross, Z. *J. Biol. Inorg. Chem.* **2001**, *6*, 733−738. (b) Aviv, I.; Gross, Z. *Chem. Commun.* **2007**, 1987−1999. (c) Gryko, D. T.; Fox, J. P.; Goldberg, D. P. *J. Porphyrins Phthalocyanines* **2004**, *8*, 1091−1105. (d) Paolesse, R. *Synlett* **2008**, *15*, 2215−2230. (e) Guilard, R.; Barbe, J. M.; Stern, C.; Kadish, K. M. In *The Porphyrin Handbook*; Kadish, K. M., Smith, K. M., Guilard, R., Eds.; Elsevier: San Diego, 2003; Vol. *18*, pp 303−349. (f) Zdilla, M. J.; Dexheimer, J. L.; Abu-Omar, M. M. *J. Am. Chem. Soc.* **2007**, *129*, 11505−11511. (g) Matsuo, T.; Hayashi, A.; Abe, M.; Matsuda, T.; Hisaeda, Y.; Hayashi, T. *J. Am. Chem. Soc.* **2009**, *131*, 15124−15125. (h) Harischandra, D. N.; Zhang, R.; Newcomb, M. *J. Am. Chem. Soc.* **2005**, *127*, 13776−13777. (i) Gross, Z.; Simkhovich, L.; Galili, N. *Chem. Commun.* **1999**, 599−600. (j) Golubkov, G.; Bendix, J.; Gray, H. B.; Mahammed, A.; Goldberg, I.; DiBilio, A. J.; Gross, Z. *Angew. Chem., Int. Ed.* **2001**, *40*, 2132−2134. (k) Liu, H. Y.; Lai, T. S.; Yeung, L. L.; Chang, C. K. *Org. Lett.* **2003**, *5*, 617−620. (l) Kumar, A.; Goldberg, I.; Botoshansky, M.; Buchman, Y.; Gross, Z. *J. Am. Chem. Soc.* **2010**, *132*, 15233−15245. (m) Gross, Z.; Gray, H. B. *Comments Inorg. Chem.* **2006**, *27*, 61−72.

(6) See ref 5h for transient absorption data that suggest the presence of an Fe(O) corrole.

(7) Fukuzumi, S.; Tokuda, Y.; Kitano, T.; Okamoto, T.; Otera, J. *J. Am. Chem. Soc.* **1993**, *115*, 8960−8968.

(8) George, G. N. *EXAFSPAK Software*; Stanford Synchrotron Radiation Laboratory, Stanford Linear Accelerator Center, Stanford University: Stanford, CA, 2000.

(9) Tenderholt, A. *PySpline*; Stanford Synchrotron Radiation Laboratory, Stanford Linear Accelerator Center, Stanford University: Stanford, CA, 2005.

(10) (a) Mustre de Leon, J.; Rehr, J. J.; Zabinsky, S. I.; Albers, R. C. *Phys. Rev. B* **1991**, *44*, 4146−4156. (b) Rehr, J. J.; Mustre de Leon, J.; Zabinsky, S. I.; Albers, R. C. *J. Am. Chem. Soc.* **1991**, *113*, 5135−5140.

(11) Badejo, I. T.; Karaman, R.; Pinkerton, A. A.; Fry, J. L. *J. Org. Chem.* **1990**, *55*, 4327−4332.

(12) (a) Stein, S. E.; Brown, R. L. *J. Am. Chem. Soc.* **1991**, *113*, 787−793. (b) Bordwell, F. G.; Cheng, J. P.; Ji, G. Z.; Satish, A. V.; Zhang, Z. M. *J. Am. Chem. Soc.* **1991**, *113*, 9790−9795. (c) Laarhoven, L. J. J.; Mulder, P.; Wayner, M. *Acc. Chem. Res.* **1999**, *32*, 342−349.

(13) Zhu, X. Q.; Li, H. R.; Li, Q.; Ai, T.; Lu, J. Y.; Yang, Y.; Cheng, J. P. *Chem.—Eur. J.* **2003**, *9*, 871−880.

(14) Lente, G.; Fabian, I.; Poe, A. J. *New J. Chem.* **2005**, *29*, 759−760.

(15) (a) Stone, K. L.; Behan, R. K.; Green, M. T. *Proc. Natl. Acad. Sci. U.S.A.* **2005**, *102*, 16563−16565. (b) Penner-Hahn, J. E.; Eble, K. S.; McMurry, T. J.; Renner, M.; Balch, A. L.; Groves, J. T.; Dawson, J. H.; Hodgson, K. O. *J. Am. Chem. Soc.* **1986**, *108*, 7819−7825. (c) Wolter, T.; Meyer-Klaucke, W.; Muther, M.; Mandon, D.; Winkler, H.; Trautwein, A. X.; Weiss, R. *J. Inorg. Biochem.* **2000**, *78*, 117−122.

(16) For an example of XAS studies with a low-spin Fe^{III} corrole, see: Hocking, R. K.; DeBeer George, S.; Gross, Z.; Walker, F. A.; Hodgson, K. O.; Hedman, B.; Solomon, E. I. *Inorg. Chem.* **2009**, *48*, 1678−1688.

(17) (a) Rohde, J. U.; Torelli, S.; Shan, X. P.; Lim, M. H.; Klinker, E. J.; Kaizer, J.; Chen, K.; Nam, W.; Que, L., Jr. *J. Am. Chem. Soc.* **2004**, *126*, 16750−16761. (b) Lim, M. H.; Rohde, J.-U.; Stubna, A.; Bukowski, M. R.; Costas, M.; Ho, R. Y. N.; Münck, E.; Nam, W.; Que, L., Jr. *Proc. Natl. Acad. Sci. U.S.A.* **2003**, *100*, 3665−3670. (c) Klinker, E. J.; Kaizer, J.; Brennessel, W. W.; Woodrum, N. L.; Cramer, C. J.; Que, L., Jr. *Angew. Chem., Int. Ed.* **2005**, *44*, 3690−3694. (d) Rohde, J.-U.; In, J.-H.; Lim, M. H.; Brennessel, W. W.; Bukowski, M. R.; Stubna, A.; Münck, E.; Nam, W.; Que, L., Jr. *Science* **2003**, *199*, 1037−1039.

(18) DeBeer George, S.; Brant, P.; Solomon, E. I. *J. Am. Chem. Soc.* **2005**, *127*, 667−674.

(19) $[(tmp)^{+\bullet}Fe^{IV}(O)(p\text{-X-PyO})]^{+}$, where tmp = tetramesitylporphyrin and *p*-Y-PyO = *para*-substituted pyridine N-oxides (Y = OCH_3, CH_3, H, or Cl).

(20) Pan, Z. Z.; Horner, J. H.; Newcomb, M. *J. Am. Chem. Soc.* **2008**, *130*, 7776−7777.

(21) (a) Bryant, J. R.; Mayer, J. M. *J. Am. Chem. Soc.* **2003**, *125*, 10351−10361. (b) Mayer, J. M. *Acc. Chem. Res.* **1998**, *31*, 441−450. (c) Wang, K.; Mayer, J. M. *J. Am. Chem. Soc.* **1997**, *119*, 1470−1471. (d) Goldsmith, C. R.; Cole, A. P.; Stack, T. D. P. *J. Am. Chem. Soc.* **2005**, *127*, 9904−9912. (e) Goldsmith, C. R.; Stack, T. D. P. *Inorg. Chem.* **2006**, *45*, 6048−6055. (f) Li, F. F.; England, J.; Que, L., Jr. *J. Am. Chem. Soc.* **2010**, *132*, 2134−2135.

(22) For an example of xanthene oxygenation by $[Mn^{V}(porph)(O)_2]^{3+}$ where a rebound mechanism is not involved, see: Arunkumar, C.; Lee, Y. M.; Lee, J. Y.; Fukuzumi, S.; Nam, W. *Chem.—Eur. J.* **2009**, *15*, 11482−11489.

(23) (a) Green, M. T. *Curr. Opin. Chem. Biol.* **2009**, *13*, 84−88. (b) Sastri, C. V.; Lee, J.; Oh, K.; Lee, Y. J.; Lee, J.; Jackson, T. A.; Ray, K.; Hirao, H.; Shin, W.; Halfen, J. A.; Kim, J.; Que, L., Jr.; Shaik, S.; Nam, W. *Proc. Natl. Acad. Sci. U.S.A.* **2007**, *104*, 19181−19186. (c) Bukowski, M. R.; Koehntop, K. D.; Stubna, A.; Bominaar, E. L.; Halfen, J. A.; Münck, E.; Nam, W.; Que, L., Jr. *Science* **2005**, *310*, 1000−1002.

(24) For examples of Mn^{V}−nitrido corroles that differ significantly in charge but do not show any difference in stability, see: (a) Saltsman, I.; Goldberg, I.; Gross, Z. *J. Porphyrins Phthalocyanines* **2010**, *14*, 615−620. (b) Golubkov, G.; Gross, Z. *J. Am. Chem. Soc.* **2005**, *127*, 3258−3259.